IEEE Access
Multidisciplinary | Rapid Review | Open Access Journal

Received June 22, 2019, accepted July 5, 2019, date of publication July 10, 2019, date of current version August 12, 2019.

Digital Object Identifier 10.1109/ACCESS.2019.2927787

Thermal Performance of the Graphene Oxide Nanofluids Flow in an Upright Channel Through a Permeable Medium

TAZA GUL[1], MALIK ZAKA ULLAH[2], ABDULLAH KHAMES ALZAHRANI[2], AND IRAJ SADEGH AMIRI[3,4]

[1]Department of Mathematics, City University of Science and Information Technology, Peshawar 25000, Pakistan
[2]Department of Mathematics, Faculty of Science, King Abdulaziz University, Jeddah 21589, Saudi Arabia
[3]Computational Optics Research Group, Advanced Institute of Materials Science, Ton Duc Thang University, Ho Chi Minh City 758307, Vietnam
[4]Faculty of Applied Sciences, Ton Duc Thang University, Ho Chi Minh City 758307, Vietnam

Corresponding author: Iraj Sadegh Amiri (irajsadeghamiri@tdtu.edu.vn)

This work was supported by the Deanship of Scientific Research (DSR), King Abdulaziz University, Jeddah, Saudi Arabia, under Grant KEP-18-130-19.

ABSTRACT The three-dimensional flow of Water based Graphene Oxide (GO-W) and Ethylene Glycol based Graphene Oxide (GO-EG) nanofluids amongst the binary upright and parallel plates is considered. The unsteady movement of the nanofluid is associated with the porous medium and the uniform magnetic field is executed in the perpendicular direction of the flow field. The basic governing equations have been altered using the Von Karman transformation, including the natural convection in the downward direction. The solution for the modeled problem has been attained by means of optimal homotopy analysis method (OHAM). The influence of the physical parameters on the momentum boundary layer, pressure, and temperature fields is mainly focused. Moreover, the comparison of the GO-W and GO-EG nanofluids under the impact of physical constraints has been analyzed graphically and numerically. The imperative physical constraints of the drag force and heat transfer rate have been computed and discussed. The results have been validated using the error analysis and the obtained outcomes have been shown and discussed. The obtained results are compared with the numerical ND-Solve method. It is obtained that the increasing order of the iterations reduces the absolute error and the results go to the strong convergence. Moreover, the impact of the physical parameters is more precise in the GO-EG nanofluid due to its higher thermophysical properties.

INDEX TERMS Water, Ethylene Glycol, Graphene Oxide, MHD, porous medium, two vertical and parallel plates, OHAM and numerical ND-solve techniques.

I. INTRODUCTION

The importance of the modern technologies and multi-tasking system in the energy sector, engineers and scientist facing diverse types of problems in which one is the joint problem of the fewer thermal efficiency of the common fluids. The low thermal conductivity of these fluids caused the thermal efficiency of the heat exchanging devices. To enhance the thermal efficiency of the base liquids and to enrich the heat transfer aspects of the devices the small sized metal (iron, steel, copper, brass) or non-metal (carbon, selenium, aluminium, sulfur) particles (1-100nm) has been used is the base fluids to execute the nanofluid. The Chinese scientist Choi [1] is the pioneer to adopt the idea of nanoparticles and its thermophysical performance. The technological importance and the utilization of nanoparticles in nanotechnology were conferred by Choi *et al.* [2].

The physical properties and homogeneous mixture of nanosized particles in the base liquids has a vital role in the preparation of nanofluid. The anticipated aspects of the nanofluids for the enhancement of thermal efficiency depend on the, thermal properties, availability, price, toxicity, adjustment to the base liquids, chemical reliability. Conceivable nanomaterials are most of the metals, carbon materials and metal oxides. Different models have been explored by the researcher based on the above-mentioned properties.

The associate editor coordinating the review of this manuscript and approving it for publication was Qiang Lai.

The thermophoretic and Brownian motion effects of the nanofluid have been examined by Buongiorno [3]. The shape of the nanosized particles rather than the spherical with new physical properties has been studied by Timofeeva *et al.* [4]. Similarly, the researchers tried to construct the suitable thermal conductivity models for the improvement of the heat exchange rate. These models are used in the field of nanotechnologies depend on the structure and behavior of the nanoparticles and base solvents. The efforts done by the researchers to define a comparative model for the improvement of the thermal conductivities. Maxwell [5], Jeffery [6], Davis [7], Lu and Lin [8] and Crosser [9] are the well-known thermal conductivity models and used in most of the mathematical models related to the problems occurring in the field of engineering and technologies.

The flow among the parallel plates is comprehensively discussed by many numbers of the researchers. They obtained the experimental and theoretical results, graphical and numerical outputs using different type of nanofluid. Sheikholeslami and Ganji [10] analyzed nanofluid flow among parallel plates under the assumption of thermophoresis and Brownian motion effects. Sheikholeslami and Ganji [11] discussed completely the effect of copper nanoparticles with water amid in parallel channels. Sheikholeslami *et al.* [12] examined the fluid flow in parallel plates and rotating system under the effect of MHD and heat source. Mahmoodi and Kandelousi [13] studied the analysis of hypothermal behavior and entropy generation under the effect of thermal radiation in a regenerative cooling. Ellahi *et al.* [14] have used the new idea to study the shape of nanoparticles in a porous medium. They mentioned the entropy analysis of the different shapes of nanosized spherical particles. To discuss cylindrical shaped particles Akber and Butt [15] presented a unique type of flow of Cu-water nanofluids using platelet-, brick and cylindrical particles. The nature of different sized nanoparticles under the influence of porous media and mixed convection is scrutinized by Ellahi *et al.* [16]. Sheikholeslami *et al.* [17] very nicely discussed and presented a fresh idea to the fluid flows among parallel plates. Mahmoodi and Kandelousi [18] discussed a comprehensive analysis of aluminium nanoparticles and kerosene oil under the influence of heat sources in parallel rotating plates.

The similarity transformations are used to simplify the basic flow equations without disturbing the physical nature of the problems. Karman [19] have used the similarity transformation for the two- and three-dimensional flow problems. To discuss more comprehensively, Sheikholeslami and Ganji [20] provide a detailed information, and take three dimensional rotating plates. Rashidi *et al.* [21] described the effect of magnetohydrodynamic in the fluid flow model. They discussed briefly the influence of $\gamma Al_2O_3 - C_2H_6O_2$ nanofluids the numerical value of physical parameters and graphical discussion section also included in their study. Ahmed *et al.* [22] fruitfully discussed $\gamma Al_2O_3 - H_2O$ and $\gamma Al_2O_3 - C_2H_6O_2$ nanofluid squeezed flow among parallel plates. Although, metal and nonmetal material have important applications and depend on their structure and properties. The carbon is the well-known material for the formation of nanofluids and heat transfer enhancement applications. The suitable base solvents for the carbon materials are water, ethylene glycol, engine oil, kerosene oil. The thermophysical properties of the base solvent water, ethylene glycol and solid material of carbon and other solid materials have been studied by the researchers in [23]–[33].

In view of the above important discussion the aim of the present work is to study the nanofluid flow of the water and ethylene glycol-based graphene oxide (GO-W/ GO-EG) nanofluid among the two parallel plates for the heat transfer enrichment applications. The medium between the plates is considered porous and the flow nature is unsteady under the influence of magnetic field.

The solution of the proposed problem has been obtained using the optimal homotopy analysis method (OHAM). Liao [34], [35] was the first person to introduce this scheme for the solution of nonlinear differential equations. He further modified this method by introducing BVPh 2.0 package to enhance the convergence of this method [36]–[40]. The 20^{th} order square residual error can easily accessible through this method as archived by Gohar *et al.* [41] and Gul *et al.* [42] and Shah *et al.* [43]. The physical and numerical outcomes have been displayed and discussed.

II. MATHEMATICAL FORMULATION

Consider the unsteady incompressible (GO-W/GO-EG) nanofluids flow amongst the two vertical plates. The medium between the plates is considered porous and the plates are settled at $y = 0$ and at $y = d$. The plates are placed vertically in the xz plane in a Cartesian coordinate system and the fluid flow is along the z axis. The y axis is perpendicular to the plates. The nanofluid flow is in the downward z direction due the existence of gravity force. The velocity components u, v, w are acting along the x, y, z directions. Assume that T_0 and T_1 are the temperatures of the plates at $y = 0$ and $y = d$. Here B_0 is represented the applied magnetic field normal to the flow path.

Keeping in mind all the upstairs supposition, the main set of equations of nanofluids between two plates are given as

$$\frac{\partial u}{\partial x} + \frac{\partial v}{\partial y} + \frac{\partial w}{\partial z} = 0, \tag{1}$$

$$\frac{\partial u}{\partial t} + u\frac{\partial u}{\partial x} + v\frac{\partial u}{\partial y} + w\frac{\partial u}{\partial z} = -\frac{1}{\rho_{nf}}\frac{\partial p}{\partial x} + \upsilon_{nf}\left(\frac{\partial^2 u}{\partial x^2} + \frac{\partial^2 u}{\partial y^2} + \frac{\partial^2 u}{\partial z^2}\right) - \frac{\upsilon_{nf}}{k}u - \frac{\sigma_{nf}B_0^2}{\rho_{nf}}u, \tag{2}$$

$$\frac{\partial v}{\partial t} + u\frac{\partial v}{\partial x} + v\frac{\partial v}{\partial y} + w\frac{\partial v}{\partial z} = -\frac{1}{\rho_{nf}}\frac{\partial p}{\partial y} + \upsilon_{nf}\left(\frac{\partial^2 \mathrm{v}}{\partial x^2} + \frac{\partial^2 \mathrm{v}}{\partial y^2} + \frac{\partial^2 \mathrm{v}}{\partial z^2}\right) - \frac{\upsilon_{nf}}{k}\mathrm{v}, \tag{3}$$

$$\frac{\partial w}{\partial t}+u\frac{\partial w}{\partial x}+\mathrm{v}\frac{\partial w}{\partial y}+w\frac{\partial w}{\partial z} = -\frac{1}{\rho_{nf}}\frac{\partial p}{\partial z}+\upsilon_{nf}\left(\frac{\partial^2 w}{\partial x^2}+\frac{\partial^2 w}{\partial y^2}+\frac{\partial^2 w}{\partial z^2}\right)-\frac{\upsilon_{nf}}{k}w-\frac{\sigma_{nf}B_0^2}{\rho_{nf}}w \quad (4)$$

$$\frac{\partial T}{\partial t}+u\frac{\partial T}{\partial x}+\mathrm{v}\frac{\partial T}{\partial y}+w\frac{\partial T}{\partial z} = \alpha_{nf}\left(\frac{\partial^2 T}{\partial x^2}+\frac{\partial^2 T}{\partial y^2}+\frac{\partial^2 T}{\partial z^2}\right). \quad (5)$$

The velocity segments are u, v and w along the x, y and z directions, T is the temperature, the acceleration due to gravity is represented by g, ρ_{nf} show the density of the solid nanoparticles, υ_{nf} show kinematic viscosity of the solid particles, p show pressure, k is the permeability, $\alpha_{nf}=\frac{k_{nf}}{(\rho C_p)_{nf}}$ is the ratio of the thermal conductivity and heat capacitance. Where electrical conductivity is represented by σ_{nf}. The set of appropriate boundary conditions are.

$$u=0,\quad \mathrm{v}=0,\ w=0,\ T=T_0\,,\ p=0\ \text{at}\ y=0, \quad (6)$$

$$u=0,\quad \mathrm{v}=-\mathrm{V},\ \ w=0,\ T=T_1\ \text{at}\ y=d. \quad (7)$$

The thermophysical constraints of the nanofluid are defined [25]:

$$\begin{aligned}\rho_{nf} &= \rho_f\,(1-\phi)+\phi\rho_s\\ \mu_{nf} &= \frac{\mu_f}{(1-\phi)^{2.5}}\\ \left(\rho C_p\right)_{nf} &= \left(\rho C_p\right)_f(1-\phi)+\left(\rho C_p\right)_s\\ \frac{k_{ns}}{k_f} &= \left(\frac{k_s+2k_f-2\phi\left(k_f-k_s\right)}{k_s+2k_f+2\phi\left(k_f-k_s\right)}\right).\end{aligned} \quad (8)$$

The Von Karman [19] similarity transformation for the proposed problems have been used as

$$\begin{aligned}u &= \frac{xU_W}{d(1-\alpha t)}f'(\eta),\quad w=\frac{d^2 g}{\nu(1-\alpha t)}h(\eta),\\ \mathrm{v} &= -\frac{U_W}{d\sqrt{1-\alpha t}}f(\eta),\\ \eta &= \frac{y}{d\sqrt{1-\alpha t}},\quad \Theta(\eta)=\frac{T-T_0}{(T_1-T_0)}.\end{aligned} \quad (9)$$

Inserting Eq. (8) into Eqs. (2-5) we obtained a system of nonlinear differential equations as:

$$\mathrm{Re}(1-\phi)^{2.5}P'-f''+Re(1-\phi)^{2.5}\left((1-\phi)+\phi\frac{\rho_s}{\rho_f}\right)\left(\frac{S}{2}\left(f+\eta f'\right)+ff'\right)+Krf=0, \quad (10)$$

$$h''+\mathrm{Re}(1-\phi)^{2.5}\left((1-\phi)+\phi\frac{\rho_s}{\rho_f}\right)\left(fh'-S\left(h+\frac{\eta}{2}h'\right)\right)-(Kr+M)(1-\phi)^{2.5}h=0, \quad (11)$$

$$\frac{k_{nf}}{k_f}\left(\eta\Theta''+2\Theta'\right)-\mathrm{Pr}\,\mathrm{Re}(1-\phi)^{-2.5}\left((1-\phi)+\phi\frac{\rho_s}{\rho_f}\right)S\left(\eta^2\Theta'+\eta\Theta\right)+\mathrm{Pr}\,\mathrm{Re}(1-\phi)^{-2.5}\left((1-\phi)+\phi\frac{\rho_s}{\rho_f}\right)\left(\eta f\Theta'+\Theta f\right)=0, \quad (12)$$

(‘) represent the differentiation. The nondimensional parameters obtained as the Reynolds number $\mathrm{Re}=\frac{U_W d}{\nu_f}$, Unsteady parameter $S=\frac{\alpha d}{U_W}$ and Prandtl number $\mathrm{Pr}=\frac{\nu_f}{\alpha_{nf}}$ respectively.

The non-dimensional pressure term p is presented as:

$$P=\frac{-\rho_f U_w}{1-\alpha t}p'. \quad (13)$$

$$\frac{df(0)}{d\eta}=0,\quad f(0)=0,\ h(0)=0,\ p(0)=0,\ \Theta(0)=0, \quad (14)$$

$$\frac{df(1)}{d\eta}=0,\quad f(1)=1,\ h(1)=0,\ \ \Theta(1)=1, \quad (15)$$

The Skin friction or the drag force $C_f=\frac{\mu_{nf}}{\rho_f U_w^2}\left(\frac{\partial u}{\partial y}+\frac{\partial w}{\partial x}\right)_{y=0}$ at the lower plate and the Nusselt number or heat transfer rate $Nu=-\frac{xk_{nf}}{k_f(T_1-T_0)}\left(\frac{\partial T}{\partial y}\right)_{y=0}$ are presented as [27]:

$$\begin{aligned}C_{fx} &= \frac{x\upsilon_f(1-\varphi)^{-2.5}}{d^2U_w(1-\alpha t)^{\frac{3}{2}}}f''(0),\\ C_{fy} &= \frac{dg(1-\varphi)^{-2.5}}{U_w(1-\alpha t)^{\frac{3}{2}}}h'(0),\end{aligned} \quad (16)$$

III. SOLUTION BY OHAM

To find an analytical solution we use OHAM procedure, Eq's (9-12) solved by a well-known and an efficient OHAM technique. OHAM procedure gives a succession solution and in the first step the trial solution is selected which satisfies the physical conditions. The trial solution for the proposed problem is obtained as:

$$\begin{aligned}f(\eta) &= -2\eta^3+3\eta^2,\quad p(\eta)=\eta,\\ h(\eta) &= \eta^2-\eta,\quad \Theta(\eta)=2\eta^2-\eta.\end{aligned} \quad (17)$$

The selected linear operators are given below

$$L_f=\frac{\partial^4 f}{\partial\eta^4},\quad L_P=\frac{\partial P}{\partial\eta},\ L_h=\frac{\partial^2 h}{\partial\eta^2},\ L_\Theta=\frac{\partial^2\Theta}{\partial\eta^2} \quad (18)$$

$$L_f\left(c_1+c_2\eta+c_3\eta^2+c_4\eta^3\right)=0,\quad L_P(c_5)=0,\quad L_h(c_6+c_7\eta)=0,\quad L_\Theta(c_8+c_9\eta)=0. \quad (19)$$

where $c_1, c_2 \ldots\ldots c_9$ are arbitrary constant which is included in general solution. k^{th}Order approximation of average residual errors is introduced by Liao [34].

$$\varepsilon_k^f\left(\hbar_f\right)=\frac{1}{N+1}\sum_{j=0}^{N}\left[\sum_{i=0}^{k}(f_i)_{\eta=j\pi\eta}\right]^2, \quad (20)$$

$$\varepsilon_k^P\left(\hbar_f,\hbar_P\right)=\frac{1}{N+1}\sum_{J=0}^{N}\left[\sum_{i=0}^{k}(f_i)_{\varsigma=j\pi\eta},\sum_{i=0}^{k}(P_i)_{\varsigma=j\pi\eta}\right]^2, \tag{21}$$

$$\varepsilon_k^h\left(\hbar_f,\hbar_h\right)=\frac{1}{N+1}\sum_{J=0}^{N}\left[\sum_{i=0}^{k}(f_i)_{\xi=j\pi\eta},\sum_{i=0}^{k}(h_i)_{\xi=j\pi\eta}\right]^2, \tag{22}$$

$$\varepsilon_k^\Theta\left(\hbar_f,\hbar_\Theta\right)=\frac{1}{N+1}\sum_{J=0}^{N}\left[\sum_{i=0}^{k}(f_i)_{\zeta=j\pi\eta},\sum_{i=0}^{k}(\Theta_i)_{\zeta=j\pi\eta}\right]^2, \tag{23}$$

$$\varepsilon^t=\varepsilon_k^f+\varepsilon_k^P+\varepsilon_k^h+\varepsilon_k^\Theta. \tag{24}$$

Here ε^t represent the total residual error. In the increasing order of approximation, the sum of the total square residual error has the tendency to rapidly converge the solution. The specified values of optimal control convergence parameters is

$$\hbar_f=-0.889633,\ \hbar_h=-0.924785,$$
$$\hbar_P=-0.000328778,\ \hbar_\Theta=-0.623565$$

in case of $Eg-GO$, while in case of Water-GO.

$$\hbar_f=-0.89084,\quad \hbar_h=-0.92862,$$
$$\hbar_P=-0.000322363,\ \hbar_\Theta=-0.597822$$

IV. RESULTS AND DISCUSSION

The two sorts of (GO-W and GO-EG) nanofluids flow amongst the two uprights and parallel plates for the heat transfer enhancement applications is analyzed in this research. The geometry of the problem is displayed in Fig.1.The solution of the problem has been obtained through OHAM technique using the BVP 2.0 package up to the 20th order approximation. The detailed discussion of the physical and numerical outputs has been deliberated in the following sections.

A. VELOCITY PROFILES

The impact of the embedded parameters over the radial and azimuthal velocity profiles for the GO-W/GO-EG nanofluids were examined physically in Figs. 2-11. Figs. 2,3 demonstrate the influence of M(magnetic parameter) versus velocity pitch $f'(\eta)\,\&\,h(\eta)$ for the GO-W and GO-EG nanofluids. It can be observed that M accelerate the motion of the fluid's downfall. This result match with the physical phenomenon since the momentum boundary layer is made of a thin layer, thus the parameter M is increased it will create a confrontation force so-called Lorentz force and this force is responsible to decrease the movement of fluid flow. The decline effect is relatively quick in the GO-W nanofluids for the larger values of M. The effect is eventual for both $f'(\eta)\,\&\,h(\eta)$ velocity profiles. The greater amount of the volume fraction ϕ increases the thermal properties of the nanofluid and the viscous forces become feeble to stop the fluid flow, also the kinetic energy of the molecules increases. Therefore, the larger values of the nanoparticle ϕ rise

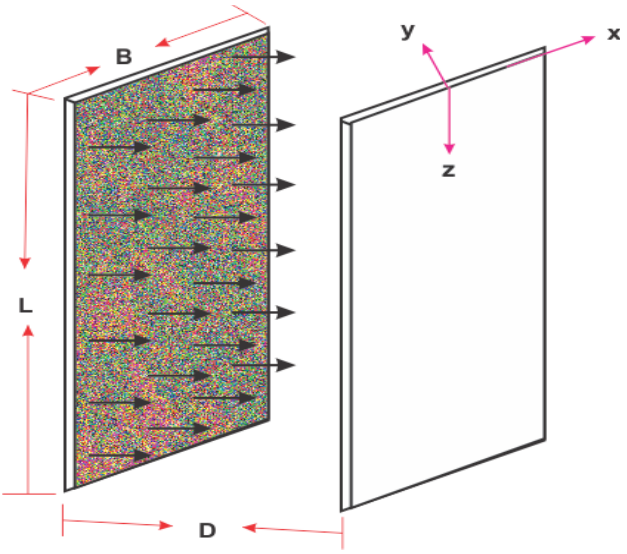

FIGURE 1. Physical sketch of the problem.

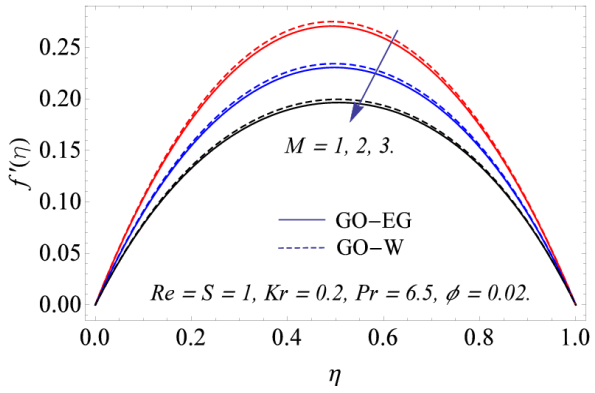

FIGURE 2. Magnetic parameter M versus $f'(\eta)$.

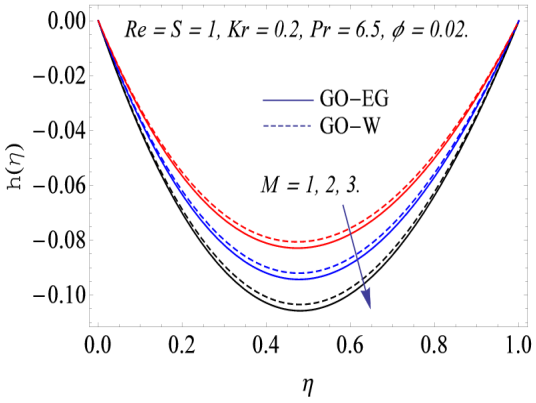

FIGURE 3. Magnet parameter M versus $h(\eta)$.

the radial and azimuthal velocities as shown in Figs. 4,5. Figs. 6,7 demonstrate the impact of the porosity constraint Kr on the velocity outlines $f'(\eta)\,\&\,h(\eta)$ comprising GO-W and GO-EG nanofluids. The larger values of Kr creating the resistive force, which goes to decrease the flow and

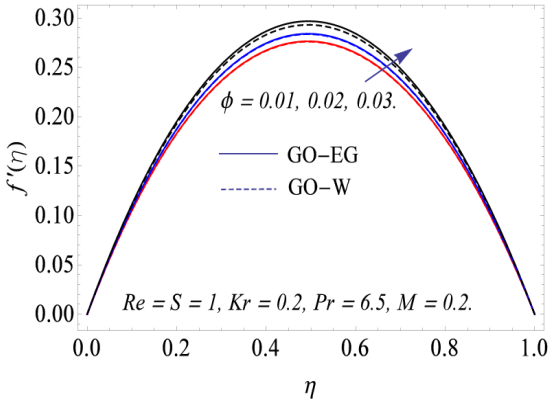

FIGURE 4. Nano particle volume fraction ϕ versus $f'(\eta)$.

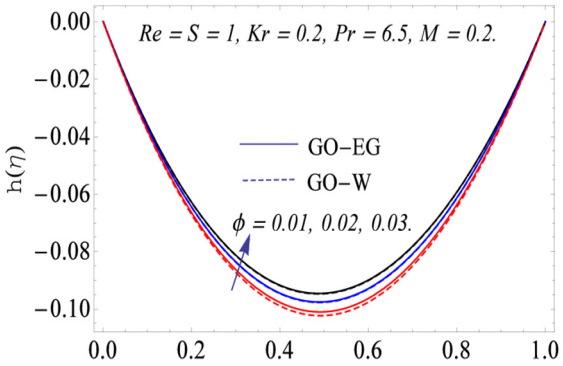

FIGURE 5. Nano particle volume fraction ϕ versus $h(\eta)$.

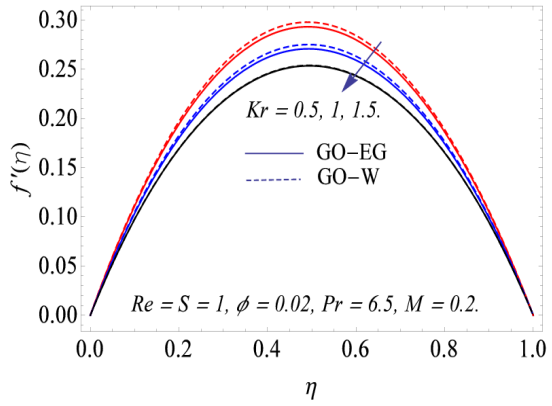

FIGURE 6. Porosity Parameter *Kr* versus $f'(\eta)$.

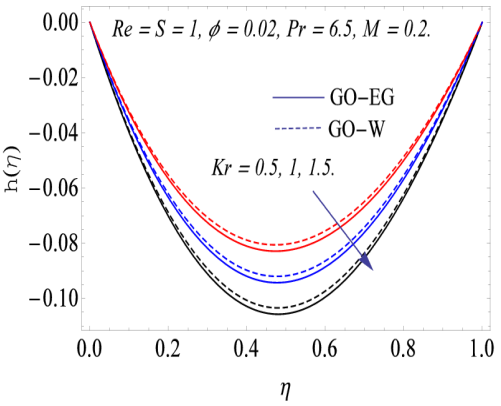

FIGURE 7. Porosity parameter *Kr* versus $h(\eta)$.

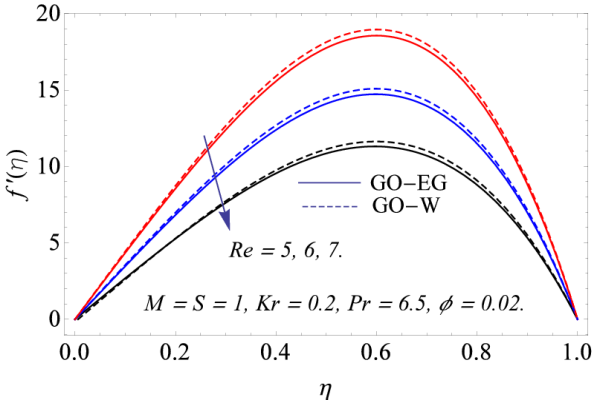

FIGURE 8. Reynolds number Re versus $f'(\eta)$.

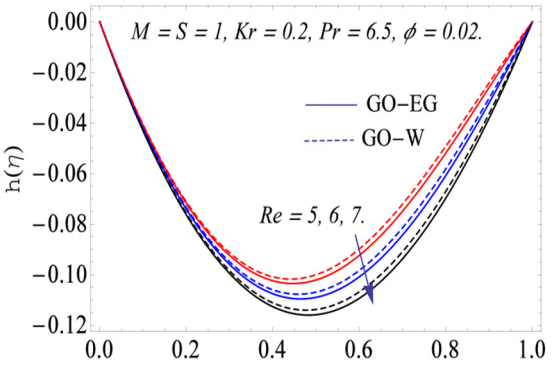

FIGURE 9. Reynolds Number Re versus $h(\eta)$.

therefore the velocity is decreased, and this effect is same for both the radial and azimuthal velocities. The influence of the Re(Reynolds number) versus $f'(\eta)\,\&\,h\,(\eta)$ velocity profiles for both sorts of GO-W and GO-EG nanofluids have been shown in Figs. 8,9. Clearly the Reynolds number is the ratio of inertial force and viscous force and by cumulative the values of Reynold number the inertial effect overcome the fluid movement and that's why *Re* decrease both velocity pitches. Further, this effect is relatively fast in the GO-W nanofluid. The effect of the unsteadiness parameter S versus velocity fields $f'(\eta)\,\&\,h\,(\eta)$ for both sorts of nanofluids GO-W and GO-EG has been displayed in Figs. 10,11. The velocity pitches diminish for the increasing value of S. In fact, greater amplitude of the unsteadiness parameter *S* increases the thickness of the momentum boundary layer and the velocity field declining. It is observed that the decreasing effect of GO-W nanofluids is comparatively slow in the radial velocity, but this effect is fast in azimuthal velocity.

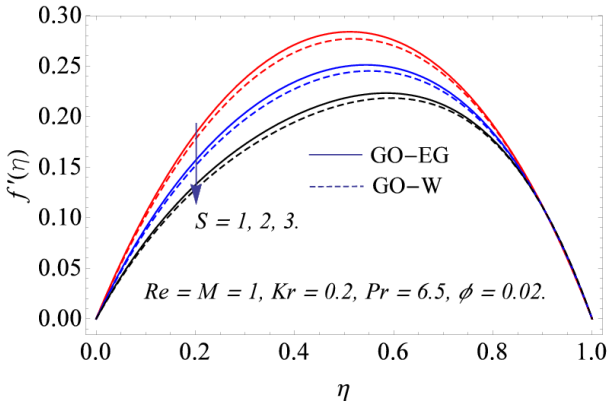

FIGURE 10. Unsteady parameter S versus $f'(\eta)$.

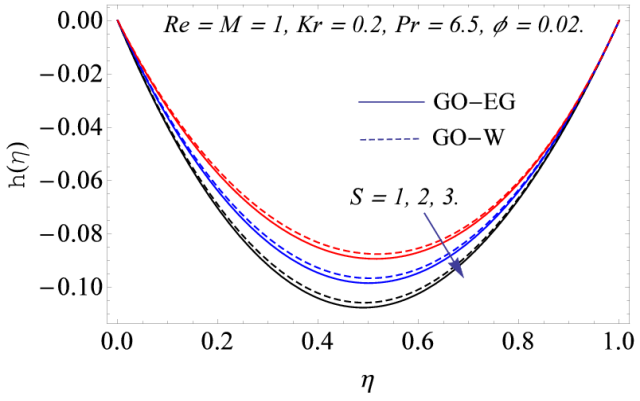

FIGURE 11. Unsteady parameter S versus $h(\eta)$.

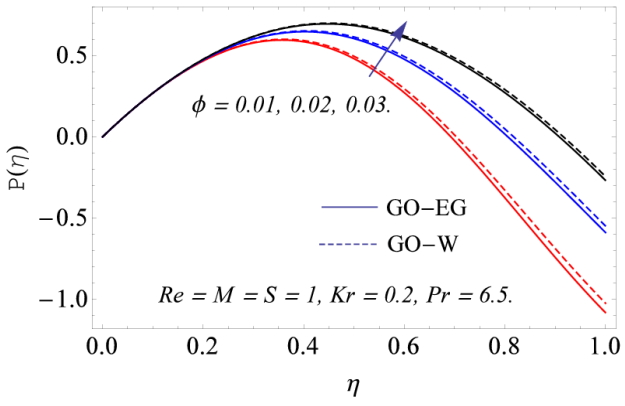

FIGURE 12. Nano particle Volume fraction ϕ versus $P(\eta)$.

B. PRESSURE PROFILES

The alteration of pressure distribution with various physical parameters of GO-W and GO-EG nanofluids has been depicted in Figs. 12-14. By raising the volume fraction the pressure profile is also augmented as revealed in Fig. 12. In fact, the concentration of the fluid, increasing with the rising value of the volume fraction ϕ and the pressure profile augmented. This effect is almost same for the GO-W and GO-EG nanofluids near the walls and comparatively larger in GO-EG in the middle. Fig. 13 display

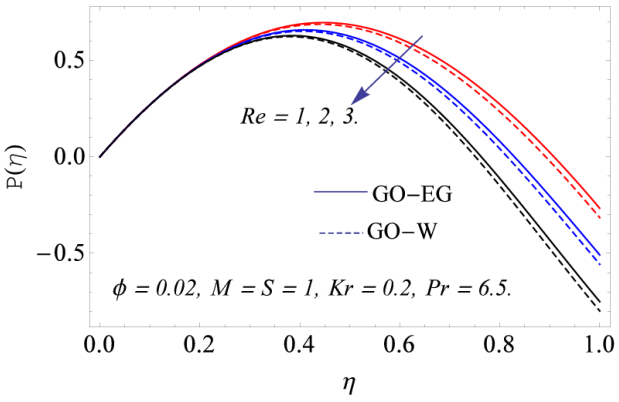

FIGURE 13. Reynolds number Re versus $P(\eta)$.

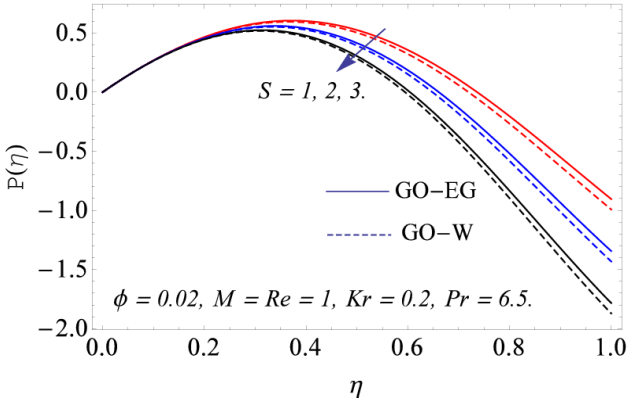

FIGURE 14. Unsteady parameter S versus $P(\eta)$.

the influence of the Reynold number versus the pressure distribution. The greater values of the Reynold number decline the pressure profile. In fact, the sturdy inertial forces of the Reynolds number decline the pressure distribution. In other words the intermolecular forces between the molecules is very high because the molecules of the fluids are tightly packed high pressure is needed to decrease the inertial forces to make the fluid in motion from rest. Again, this effect is comparatively faster in GO-EG nanofluid in the middle of the walls.

Fig.14 shows the result of unsteady parameter S, versus the pressure profile and no doubt to mention that for larger value of S the pressure field is decreasing, the reason behind this for larger value of S the momentum boundary layer thickness increasing the collision between the molecules is increased due to this process pressure profile is decreased and this effect is quicker utilizing in the GO-EG nanofluid as compared to the GO-W nanofluid. In short way, the thermal conductivity of GO-EG nanofluid is stronger than the GO-W nanofluids and as a result the viscous forces become feeble with the larger amount of the unsteadiness.

C. TEMPERATURE PROFILE

The changes in temperature field with different embedded parameters of GO-W and GO-EG nanofluids have been

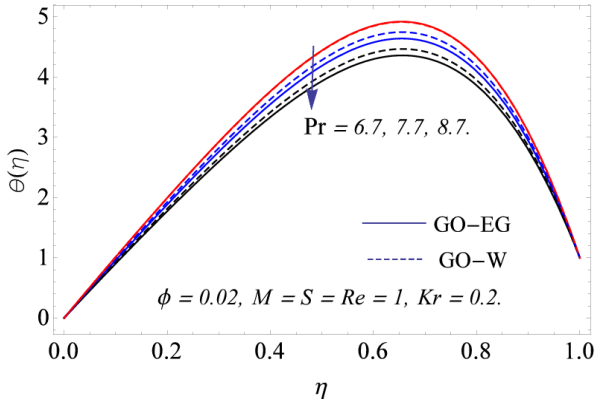

FIGURE 15. Prandtl number Pr versus Θ(η).

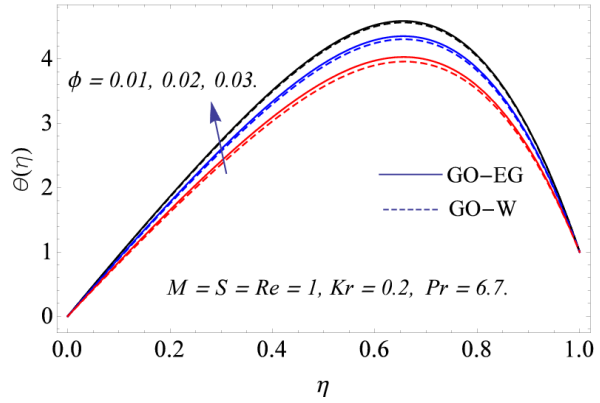

FIGURE 16. Nano particle Volume fraction ϕ versus Θ(η).

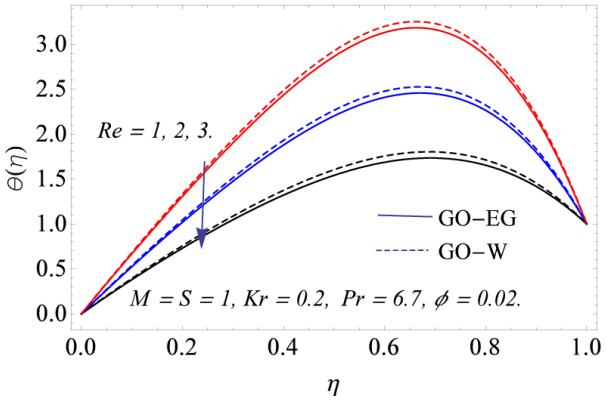

FIGURE 17. Reynolds number Re versus Θ(η).

depicted in Figs. 15-18. Fig.15 depicts the temperature field for varying values of Prandtl number Pr in the existence of GO-W and GO-EG nanofluids. It is obvious that Pr enhances due to decelerating the thermal boundary layer. The decline effect is relatively strong in GO-EG nanofluid as compared to GO-W nanofluid. Fig. 16 shows the variation in the temperature field with the fluctuation in the volume fraction ϕ. Temperature field increases due to the rising value of ϕ for both sorts of GO-W and GO-EG nanofluids. Fig.17 depicts

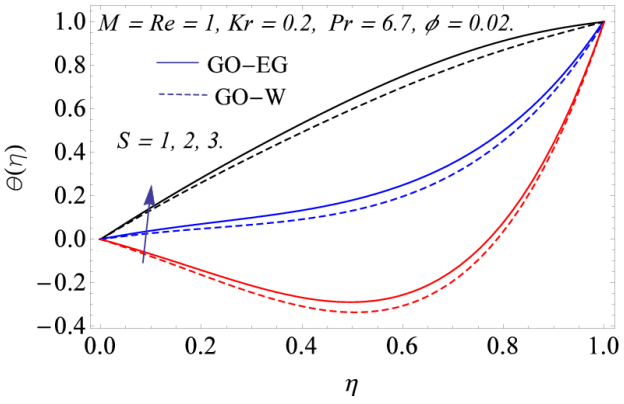

FIGURE 18. Unsteady parameter *S* versus Θ(η).

TABLE 1. The experimental value of the base solvents and material are [25], [26].

Model	$\rho\left(kg/m^3\right)$	$Cp(J/kgK)$	$K(W/mk)$
water	997.1	4179	0.613
Graphene oxide (GO)	1800	717	5000
Ethylene Glycol (EG)	1.115	0.58	0.1490

that by raising Reynold number temperature pitch is decreasing in the presence of GO-W and GO-EG nanofluids. In fact, the inertial forces improved with the excess of Reynolds number and as a result the cooling effect increases to reduce the thermal boundary layer. In other words, the strong inertial forces strengthen, the inter molecular forces and the atoms of the fluid are becoming closely pack due to strong chemical bonds between atom and molecules extra energy is needed to break the bond. The strong thermal conductivity of GO-EG nanofluid the cooling effect is relatively faster in GO-W nanofluid and the temperature profile decline quickly for more values of Re utilizing GO-W nanofluid. Fig.18 witnesses the influence of unsteadiness parameter in the temperature profile. It is noticed that by growing the value of unsteadiness constraint, the temperature field accelerating for larger values of S under the consideration of GO-W and GO-EG nanofluids.

V. TABLES DISCUSSION

The experimental values of the base solvents and materials revealed in Table.1. Tables 2, 3 represent the individual's

TABLE 2. The sum of the total squared residual errors for $GO-W$.When $Pr = 6.7, Kr = M = S = Re = 0.1, \phi = 0.03$.

m	$\varepsilon_m^f\ GO-W$	$\varepsilon_m^h\ GO-W$	$\varepsilon_m^P\ GO-W$	$\varepsilon_m^\Theta GO-W$
6	1.54×10^{-6}	7.97×10^{-9}	2.93×10^{-7}	2.97×10^{-3}
12	2.66×10^{-13}	6.33×10^{-16}	2.37×10^{-7}	3.21×10^{-7}
18	7.34×10^{-20}	1.30×10^{-22}	2.37×10^{-7}	8.73×10^{-12}
24	2.71×10^{-26}	3.93×10^{-29}	2.37×10^{-7}	4.52×10^{-16}
30	1.42×10^{-29}	1.11×10^{-33}	2.37×10^{-7}	1.90×10^{-20}

TABLE 3. The sum of the total squared residual errors for $GO-EG$ when $Pr = 6.7, Kr = M = S = Re = 0.1, \phi = 0.03$.

m	$\varepsilon_m^f\ GO$ EG	$\varepsilon_m^h\ GO$ EG	$\varepsilon_m^P\ GO$ EG	$\varepsilon_m^\Theta GO$ EG
6	1.60×10^{-6}	8.81×10^{-9}	3.06×10^{-6}	3.66×10^{-3}
12	2.90×10^{-13}	7.32×10^{-16}	2.47×10^{-7}	5.04×10^{-7}
18	8.37×10^{-20}	1.55×10^{-22}	2.47×10^{-7}	1.70×10^{-11}
24	3.07×10^{-26}	5.03×10^{-29}	2.47×10^{-7}	1.17×10^{-15}
30	2.26×10^{-32}	5.43×10^{-33}	2.47×10^{-7}	6.08×10^{-20}

TABLE 4. Impact of the physical parameters versus $-f''(0)$.

Re	S	Kr	$f''(0)\ GO-W$	$f''(0)GO-EG$
0.1	0.9	0.8	6.22547	6.46264
0.2			6.81442	7.55048
	0.8		6.19352	6.41735
	0.7		6.16159	6.3721
		0.9	6.20244	6.42399
		1.0	6.17947	6.3855

average square residual error of Ethylene Glycol-Graphene Oxide and Water-Graphene Oxide executed in a different order of approximation. We also noticed that average square residual error value can be reduced by increasing the order of approximation.

TABLE 5. Impact of the physical parameters versus $-h'(0)$.

Re	S	Kr	$-h'(0)\ GO-W$	$-h'(0)\ GO-EG$
0.1	0.9	0.8	0.201661	0.201677
0.2			0.198593	0.198602
	0.8		0.201944	0.201907
	0.7		0.202228	0.202193
		0.9	0.198869	0.198833
		1.0	0.196102	0.196069

TABLE 6. Impact of the physical parameters versus heat transfer rate $\Theta'(0)$.

S	Pr	ϕ	$\Theta'(0)GO-W$	$\Theta'(0)GO-EG$
0.9	0.7	0.01	1.84951	1.84066
0.8			1.85055	1.84169
0.7			1.85159	1.84271
	0.8		1.84967	1.84085
	0.9		1.84983	1.84104
		0.02	1.86498	1.84688
		0.03	1.85387	1.83477

In Table 4, 5 the impact of the various physical parameters versus skin fractions $f''(0)\& -h'(0)$ have been examined. The larger value of Re improving the inertial effect and as a result the $f''(0)$ increases. Further, this effect is relatively fast in the GO-EG nanofluid while in Table 5 the skin fraction $-h'(0)$ declines and this effect is more appropriate in $GO-W$ nanofluid as compared to $GO-EG$ nanofluid.

In Table 4 the declining values of the unsteady parameter S reduce the skin friction $f''(0)$ while for the same values of S in Table 5 enhances the skin friction $-h'(0)$. The larger values of Kr decline the skin frictions $f''(0)\&-h'(0)$ as shown in Tables 4,5 for both types of nanofluids $GO-W/GO-EG$ nanofluids respectively.

Table 6. Represent heat transfer rate, Physically the larger amount of nanoparticle volume fraction utilized for the heat transfer enhancement. Therefore, the rising values of ϕ decline the cooling effect. Similarly, the increasing values of the unsteady parameter S increasing the temperature field while its decreasing values enhancing the heat transfer rate as shown in Table. 6. The temperature field decreases with larger amount of Prandtl value and cooling effect improves as depicted in Table. 6.

The comparison of OHAM and Numerical (ND-Solve) methods have been displayed for the GO-EG and GO-W nanofluids in Tables 7, 8. Clearly, the increasing number of iterations reduces the absolute error between the two methods. The increasing number of iterations of the numerical

TABLE 7. OHAM and Numerical comparison results for *GO − EG* When Pr = 0.7, Re = 0.4, M = 0.2, Kr = 1, $\varphi = 0.01$, S = 0.9.

N0.	*OHAM*	*Numerical*	Absolute Error
1.	3.21×10^{-11}	4.62×10^{-28}	3.11×10^{-11}
2	3.61×10^{-11}	1.09×10^{-28}	3.64×10^{-11}
3	4.67×10^{-10}	1.37×10^{-28}	4.68×10^{-10}
4	4.29×10^{-10}	1.57×10^{-28}	4.47×10^{-10}
5	3.56×10^{-10}	1.38×10^{-28}	3.58×10^{-10}
6	2.10×10^{-10}	1.27×10^{-28}	2.12×10^{-10}

TABLE 8. OHAM and Numerical comparison results for *GO − W*. When Pr = 0.7, Re = 0.4, M = 0.2, Kr = 1, $\varphi = 0.01$, S = 0.9.

No	OHAM	Numerical	Error
1.	3.11×10^{-11}	2.23×10^{-28}	3.11×10^{-11}
2	4.73×10^{-10}	1.57×10^{-28}	4.73×10^{-10}
3	4.48×10^{-10}	1.69×10^{-28}	4.48×10^{-10}
4	3.60×10^{-10}	1.45×10^{-28}	3.60×10^{-10}
5	2.19×10^{-10}	1.35×10^{-28}	2.19×10^{-10}
6	1.07×10^{-10}	1.21×10^{-28}	1.07×10^{-10}

method and increasing order of the approximations of the OHAM method reduces the absolute error and the results approach towards the strong convergence.

VI. CONCLUSION

In current article we examine, unsteady incompressible MHD 3D water and ethylene glycol-based graphene oxide nanofluid flow passed through a permeable medium limited by two vertical plates. The two types of nanofluids (GO-W) and (GO-EG) have been used in the mathematical model for the heat transfer enhancement applications. The governing equations have been altered into the set of nonlinear differential equations by using the Von-Karman transformations. The proposed problem is solved by the well-known OHAM method for the velocity profiles, pressure distribution and temperature profile. The numerical ND-Solve method has been used for the validation of the obtained results through OHAM.

The main outputs of the problem are pointed out as:

1) Radial and azimuthal velocity profiles depreciated with the larger values of the magnetic field M, porosity parameter Kr, unsteady parameter S, Reynold number Re.
2) The radial and azimuthal velocity pitches are increasing with the rising value of the volume fraction ϕ.
3) Temperature distribution running down to Prandtl number Pr, Reynold number Re and running up for volume fraction ϕ.
4) Pressure profile is diminished for Reynold number Re, unsteady parameter S and rises with greater volume fraction ϕ.
5) The increasing number of iterations of the numerical method and increasing order of the approximations of the OHAM method reduces the absolute error and the results approach towards the strong convergence.
6) Overall, it has been concluded that the GO-EG nanofluid comparatively stronger thermal efficiency than the GO-W nanofluids.

NOMENCLATURE

B_0	Magnetic field strength (NmA^{-1})
C_f	Skin friction coefficient
c_p	Specific heat $(Jkg^{-1}K^{-1})$
k_{nf}	Permeability of the nanofluids
α_{nf}	Ratio of thermal conductivity and Heat Capacitance
f, h	Dimensional velocity profiles
U_w	Stretched velocity
T_0	Temperature at a plate (K)
T_1	Temperature away from plate (K)
P	Pressure
Kr	Porosity parameter
Nu_x	Nusselt number
GO	Graphene oxide
EG	Ethylene glycol
Pr	Prandtl number
M	Magnetic parameter
Re_x	Local Reynolds number
g	Gravitational acceleration
S	Unsteady Parameter
T	Fluid temperature (K)
W	Water
u, v, w	Velocity components (ms^{-1})
x, y, z	Coordinate axis
$C_i (i = 1 - 10)$	Constants
Greek Letters	
Θ	Dimensional heat profile
ϕ	Solid nanoparticles volume fraction
η	Similarity variable
ν_{nf}	Kinematic viscosity of nanofluids (m^2s^{-1})
μ_{nf}	Viscosity of the nanofluid (m^2s^{-1})
ρ_{nf}	Density of the nanofluids (Kgm^{-3})
σ_{nf}	Electrical conductivity (Sm^{-1})

ACKNOWLEDGMENT

This project was funded by the Deanship of Scientific Research (DSR) at King Abdulaziz University, Jeddah, under

grant no. KEP-18-130-39. The authors, therefore, acknowledge with thanks DSR for technical and financial support.

REFERENCES

[1] S. U. S. Choi, D. A. Singer, and H. P. Wang, "Developments and applications of non-Newtonian flows," *ASME FED*, vol. 66, pp. 99–105, Nov. 1995.
[2] S. U. S. Choi, Z. G. Zhang, W. Yu, F. E. Lockwood, and E. A. Grulke, "Anomalous thermal conductivity enhancement in nanotube suspensions," *Appl. Phys. Lett.*, vol. 79, no. 14, pp. 2252–2254, 2001.
[3] J. Buongiorno, "Convective transport in nanofluids," *J. Heat Transf.*, vol. 128, no. 3, pp. 240–250, 2006.
[4] E. V. Timofeeva, J. L. Routbort, and D. Singh, "Particle shape effects on thermophysical properties of alumina nanofluids," *J. Appl. Phys.*, vol. 106, no. 1, 2009, Art. no. 014304.
[5] J. C. Maxwell, *A Treatise on Electricity and Magnetism*, vol. 1. Oxford, U.K.: Clarendon, 1881.
[6] D. J. Jeffrey, "Conduction through a random suspension of spheres," *Proc. Roy. Soc. London A, Math. Phys. Sci.*, vol. 335, pp. 355–367, Nov. 1973.
[7] R. H. Davis, "The effective thermal conductivity of a composite material with spherical inclusions," *Int. J. Thermophys.*, vol. 7, no. 3, pp. 609–620, 1986.
[8] S.-Y. Lu and H.-C. Lin, "Effective conductivity of composites containing aligned spheroidal inclusions of finite conductivity," *J. Appl. Phys.*, vol. 79, no. 9, pp. 6761–6769, 1996.
[9] R. L. Hamilton and O. K. Crosser, "Thermal conductivity of heterogeneous two-component systems," *Ind. Eng. Chem. Fundam.*, vol. 1, no. 3, pp. 187–191, 1962.
[10] M. Sheikholeslami and D. D. Ganji, "Nanofluid flow and heat transfer between parallel plates considering Brownian motion using DTM," *Comput. Methods Appl. Mech. Eng.*, vol. 283, pp. 651–663, Jan. 2015.
[11] M. Sheikholeslami and D. D. Ganji, "Heat transfer of Cu-water nanofluid flow between parallel plates," *Powder Technol.*, vol. 235, pp. 873–879, Feb. 2013.
[12] M. Sheikholeslami, M. Hatami, and D. D. Ganji, "Nanofluid flow and heat transfer in a rotating system in the presence of a magnetic field," *J. Mol. Liquids*, vol. 190, pp. 112–120, Feb. 2014.
[13] M. Mahmoodi and S. Kandelousi, "Analysis of the hydrothermal behavior and entropy generation in a regenerative cooling channel considering thermal radiation," *Nucl. Eng. Des.*, vol. 291, pp. 277–286, Sep. 2015.
[14] R. Ellahi, M. Hassan, and A. Zeeshan, "Shape effects of nanosize particles in Cu–H_2O nanofluid on entropy generation," *Int. J. Heat Mass Transf.*, vol. 81, pp. 449–456, Feb. 2015.
[15] N. S. Akbar and A. W. Butt, "Ferromagnetic effects for peristaltic flow of Cu–water nanofluid for different shapes of nanosize particles," *Appl. Nanosci.*, vol. 6, no. 3, pp. 379–385, 2016.
[16] R. Ellahi, M. Hassan, A. Zeeshan, and A. A. Khan, "The shape effects of nanoparticles suspended in HFE-7100 over wedge with entropy generation and mixed convection," *Appl. Nanosci.*, vol. 6, no. 5, pp. 641–651, 2016.
[17] M. Sheikholeslami, M. M. Rashidi, D. M. Al Saad, F. Firouzi, H. B. Rokni, and G. Domairry, "Steady nanofluid flow between parallel plates considering thermophoresis and Brownian effects," *J. King Saud Univ.-Sci.*, vol. 28, no. 4, pp. 380–389, 2016.
[18] M. Mahmoodi and S. Kandelousi, "Application of DTM for kerosene-alumina nanofluid flow and heat transfer between two rotating plates," *Eur. Phys. J. Plus*, vol. 130, no. 7, p. 142, 2015.
[19] T. V. Karman, "Über laminare und turbulente Reibung," *ZAMM-J. Appl. Math. Mech.*, vol. 1, no. 4, pp. 233–252, 1921.
[20] M. Sheikholeslami and D. D. Ganji, "Three dimensional heat and mass transfer in a rotating system using nanofluid," *Powder Technol.*, vol. 253, pp. 789–796, Feb. 2014.
[21] M. M. Rashidi, N. V. Ganesh, A. A. Hakeem, B. Ganga, and G. Lorenzini, "Influences of an effective Prandtl number model on nano boundary layer flow of γ Al_2O_3–H_2O and γ Al_2O_3–$C_2H_6O_2$ over a vertical stretching sheet," *Int. J. Heat Mass Transf.*, vol. 98, pp. 616–623, Jul. 2016.
[22] N. Ahmed, U. Khan, and S. T. Mohyud-Din, "Influence of an effective Prandtl number model on squeezed flow of γ Al_2O_3-H_2O and γ Al_2O_3-$C_2H_6O_2$ nanofluids," *J. Mol. Liquids*, vol. 238, pp. 447–454, Jul. 2017.
[23] T. Gul and K. Firdous, "The experimental study to examine the stable dispersion of the graphene nanoparticles and to look at the GO–H_2O nanofluid flow between two rotating disks," *Appl. Nanosci.*, vol. 8, no. 7, pp. 1711–1727, 2018.
[24] S. Aman, I. Khan, Z. Ismail, M. Z. Salleh, and Q. M. Al-Mdallal, "Heat transfer enhancement in free convection flow of CNTs Maxwell nanofluids with four different types of molecular liquids," *Sci. Rep.*, vol. 7, no. 1, 2017, Art. no. 2445.
[25] M. Azimi, A. Azimi, and M. Mirzaei, "Investigation of the unsteady graphene oxide nanofluid flow between two moving plates," *J. Comput. Theor. Nanosci.*, vol. 11, no. 10, pp. 2104–2108, 2014.
[26] Y. Gao, H. Wang, A. P. Sasmito, and A. S. Mujumdar, "Measurement and modeling of thermal conductivity of graphene nanoplatelet water and ethylene glycol base nanofluids," *Int. J. Heat Mass Transf.*, vol. 123, pp. 97–109, Aug. 2018.
[27] S. T. Mohyud-Din, S. I. Khan, and B.-B. Mohsin, "Velocity and temperature slip effects on squeezing flow of nanofluid between parallel disks in the presence of mixed convection," *Neural Comput. Appl.*, vol. 28, no. 1, pp. 169–182, 2017.
[28] M. Suleman, M. Ramzan, S. Ahmad, D. Lu, M. Taseer, and J. D. Chung, "A numerical simulation of silver–water nanofluid flow with impacts of newtonian heating and homogeneous–heterogeneous reactions past a nonlinear stretched cylinder," *Symmetry*, vol. 11, no. 2, p. 295, 2019.
[29] I. Khan and M. A. Alqahtani, "MHD nanofluids in a permeable channel with porosity," *Symmetry*, vol. 11, no. 2, p. 378, 2019.
[30] R. Ellahi, A. Zeeshan, F. Hussain, and T. Abbas, "Two-phase couette flow of couple stress fluid with temperature dependent viscosity thermally affected by magnetized moving surface," *Symmetry*, vol. 11, no. 5, p. 647, 2019.
[31] R. Ellahi, M. Hassan, and A. Zeeshan, "Study of natural convection MHD nanofluid by means of single and multi-walled carbon nanotubes suspended in a salt-water solution," *IEEE Trans. Nanotechnol.*, vol. 14, no. 4, pp. 726–734, Jun. 2015.
[32] R. Ellahi, "The effects of MHD and temperature dependent viscosity on the flow of non-Newtonian nanofluid in a pipe: Analytical solutions," *Appl. Math. Model.*, vol. 37, no. 3, pp. 1451–1457, 2013.
[33] R. Ellahi, A. Zeeshan, F. Hussain, and T. Abbas, "Study of shiny film coating on multi-fluid flows of a rotating disk suspended with nano-sized silver and gold particles: A comparative analysis," *Coatings*, vol. 8, no. 12, p. 422, 2018.
[34] S. J. Liao, "The proposed homotopy analysis technique for the solution of nonlinear problems," Ph.D. dissertation, Shanghai Jiao Tong Univ., Shanghai, China, 1992.
[35] S. Liao, "On the homotopy analysis method for nonlinear problems," *Appl. Math. Comput.*, vol. 147, no. 2, pp. 499–513, 2004.
[36] S. Liao, "An optimal homotopy-analysis approach for strongly nonlinear differential equations," *Commun. Nonlinear Sci. Numer. Simul.*, vol. 15, no. 8, pp. 2003–2016, 2010.
[37] S. Liao, Ed., *Advances in the Homotopy Analysis Method*. Singapore: World Scientific, 2013, ch. 7.
[38] Z. Barikbin, R. Ellahi, and S. Abbasbandy, "The Ritz-Galerkin method for MHD Couette flow of non-Newtonian fluid," *Int. J. Ind. Math.*, vol. 6, pp. 235–243, May 2014.
[39] T. Hayat, R. S. Saif, R. Ellahi, T. Muhammad, and B. Ahmad, "Numerical study of boundary-layer flow due to a nonlinear curved stretching sheet with convective heat and mass conditions," *Results Phys.*, vol. 7, pp. 2601–2606, Jan. 2017.
[40] T. Hayat, R. S. Saif, R. Ellahi, T. Muhammad, and B. Ahmad, "Numerical study for Darcy-Forchheimer flow due to a curved stretching surface with Cattaneo-Christov heat flux and homogeneous-heterogeneous reactions," *Results Phys.*, vol. 7, pp. 2886–2892, Jan. 2017.
[41] G. Taza, K. Waris, S. Muhammad, A. K. Muhammad, and B. Ebenezer, "MWCNTs/SWCNTs nanofluid thin film flow over a nonlinear extending disc: OHAM solution," *J. Therm. Sci.*, vol. 28, no. 1, pp. 115–122, 2018.
[42] T. Gul, I. Haleem, I. Ullah, M. A. Khan, E. Bonyah, I. Khan, and M. Shuaib, "The study of the entropy generation in a thin film flow with variable fluid properties past over a stretching sheet," *Adv. Mech. Eng.*, vol. 10, no. 11, pp. 1–15, 2018.
[43] Z. Shah, A. Dawar, O. A. Alzahrani, A. J. Khan, and S. Islam, "Hall effect on couple stress 3D nanofluid flow over an exponentially stretched surface with Cattaneo Christov heat flux model," *IEEE Access*, vol. 7, pp. 64844–64855, 2019. doi: 10.1109/ACCESS.2019.2916162.

TAZA GUL received the M.Sc. degree from Quaid-i-Azam University, Islamabad, Pakistan, the MPhil degree from Islamia College University, Peshawar, Pakistan, and the Ph.D. degree from Abdul Wali Khan University Mardan, Pakistan. He is currently with the Higher Education Department, Khyber Pakhtunkhwa, and an Associate Professor (Adjunct Professor) with the City University of Science and Information Technology, Peshawar, Pakistan. He has written more than 100 papers and books in various filed of mechanical engineering and bio mathematics. His research interests include nanofluid, CFD, simulation, heat transfer, MHD, fractional calculus, mesoscopic modeling, nonlinear science, magnetohydrodynamic, bio fluids, and bio mathematics.

MALIK ZAKA ULLAH received the M.Sc. degree in computational mathematics from the Blekinge Institute of Technology, Sweden, and the Ph.D. degree in computational mathematics from the University of Insubria, Italy. He is currently an Assistant Professor with the Department of Mathematics, King Abdulaziz University, Saudi Arabia. His research interests include nonlinear equation solvers, numerical linear algebra, iterative methods, nonlinear optics, and computational fluid dynamics.

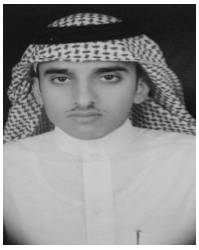

ABDULLAH KHAMES ALZAHRANI received the M.Sc. and Ph.D. degrees in mathematics from Heriot-Watt University, U.K. He is currently an Associate Professor with the Department of Mathematics, King Abdulaziz University, Saudi Arabia. His research interests include bio mathematics, numerical analysis for partial differential equations, and computational fluid dynamics.

IRAJ SADEGH AMIRI received the M.S. and Ph.D. degrees in physics from the University of Technology Malaysia (UTM). He is currently a Senior Researcher in photonics with Ton Duc Thang University (TDTU), Vietnam. He has authored or coauthored more than 100 international peer reviewed journals. His main research interests include modeling plasmonic photonics devices and plasmonics photonics devices, including device design fabrications and testing.